Coherent effects in the scattering of light from two-dimensional rough metal surfaces

Paul Anton Letnes,[1,2] Tor Nordam,[1,*] and Ingve Simonsen[1,3]

[1]*Department of Physics, The Norwegian University of Science and Technology (NTNU), Trondheim NO-7491, Norway*
[2]*e-mail: paul.anton.letnes@gmail.com*
[3]*e-mail: Ingve.Simonsen@ntnu.no*
**Corresponding author: tor.nordam@gmail.com*

Received January 31, 2013; accepted March 4, 2013;
posted April 19, 2013 (Doc. ID 184614); published May 14, 2013

We investigate numerically multiple light-scattering phenomena for two-dimensional randomly rough metallic surfaces, where surface plasmon polaritons (SPPs) mediate several surface scattering effects. The scattering problem is solved by numerical solution of the reduced Rayleigh equation for reflection. The multiple scattering phenomena of enhanced backscattering and enhanced forward scattering are observed in the same system, and their presence is due to the excitation of SPPs. The numerical results discussed are qualitatively different from previous results for one-dimensionally rough surfaces, as one-dimensional surfaces have a limited influence on the polarization of light.

OCIS codes: (290.1483) BSDF, BRDF, and BTDF; (290.4210) Multiple scattering; (290.5825) Scattering theory; (290.5880) Scattering, rough surfaces.
http://dx.doi.org/10.1364/JOSAA.30.001136

1. INTRODUCTION

A hot topic in the electronics and photonics community is plasmonics, due to the prediction that surface plasmon polaritons (SPPs) can carry information faster and with less energy loss than electronic circuits [1]. SPPs can have a penetration depth in metal on the order of 10 nm, that is, two-orders of magnitude smaller than the wavelength of visible light in vacuum. This means that plasmonics allows light to be concentrated and manipulated by structures well below the diffraction limit from classical optics.

SPP excitation is also being investigated as a way to improve the performance of photovoltaic devices. For thin solar cells, with a thickness on the order of 1 μm, the path length of light traveling through the cell is insufficient to absorb more than a small fraction of the incident energy. By converting light into SPPs, which can propagate along the dielectric–metal interface at the back of the photovoltaic cell, it is possible to absorb a larger fraction of the incident energy [2].

Because SPPs propagate along the interface of a metal, they are sensitive to conditions on the surface, making SPPs well suited for sensor applications. Such devices are often called surface plasmon resonance sensors, and can be used, for example, for microarray analysis of proteins [3] or DNA [4].

At a flat interface, incident light cannot couple to SPPs due to momentum mismatch. By manipulating the surface roughness, however, it is possible to control the coupling of incident light into SPPs. In this paper, we consider light reflected from randomly rough surfaces with particular statistical properties and study the multiple scattering phenomena that arise due to SPPs. Several multiple scattering phenomena have been predicted theoretically and/or confirmed experimentally. For example, enhanced backscattering was predicted by McGurn *et al.* [5] and later confirmed experimentally by West and O'Donnell [6]. The enhanced backscattering phenomenon is a double scattering phenomenon caused by constructive interference between a wave scattered (at least) twice by the surface and its time-reversed partner. The excitation of SPPs is usually involved in this process. For weak (low rms) surface roughness, scattering processes are usually dominated by single scattering, which may mask higher-order scattering contributions. Hence, West and O'Donnell designed a surface whose roughness had a power spectrum that suppresses single scattering in a certain angular interval, allowing multiple scattering effects to be seen more clearly [6]. The surface in question had a surface profile function dependent on only one of the axes in the surface plane; colloquially, we refer to such surfaces as "one-dimensional." This power spectrum is now known as the West–O'Donnell spectrum or the rectangular spectrum.

Enhanced forward scattering was first predicted theoretically by O'Donnell [7], who termed it the enhanced specular peak phenomenon [8]. O'Donnell investigated the scattering of light from surfaces with weak, one-dimensional roughness by the use of perturbation theory and reported an enhancement in the specular direction of the intensity of the light scattered diffusely by the rough surface. To lowest order in the surface profile function, this phenomenon appears as an eight-order contribution to the intensity within small-amplitude perturbation theory, and for one-dimensional surface roughness it is caused by constructive interference between *counterpropagating* SPPs; see Fig. 10 [7]. To confirm these findings, O'Donnell and Mendéz subsequently studied surface scattering from one-dimensional surfaces by direct solution of the one-dimensional reduced Rayleigh equation [9]. Their findings were later confirmed by Simonsen [10], who also performed a detailed numerical study of this

phenomenon, focusing on the competition between how light couples into and out from SPPs and how one SPP can couple to another counterpropagating SPP.

Up till now, the enhanced forward scattering phenomenon has not been studied for two-dimensional randomly rough surfaces either by perturbation theory or by computer simulations. Moreover, only a few numerical studies of enhanced backscattering have appeared in the literature for two-dimensional roughness. In this paper, we investigate light scattering from two-dimensionally rough surfaces by means of large-scale computer simulations, with a focus on phenomena caused by the excitation and interference of SPPs. In particular, we are interested in the enhanced backscattering phenomenon and the less-studied phenomenon of forward scattering enhancement. The understanding of such phenomena could be useful for the understanding and controlling of light–plasmon coupling in plasmonic circuits. Furthermore, two-dimensional surface roughness leads to significant polarization effects that cannot be taken into account in a one-dimensional model.

This paper is organized as follows. In Section 2, we discuss the relevant theory, including how the statistical properties of the surface roughness decide which scattering processes are allowed. Section 3 presents results from numerical simulations, exhibiting enhanced forward scattering and enhanced backscattering. Finally, concluding remarks are presented in Section 4.

2. THEORY

The system under study consists of a metallic substrate in vacuum [Fig. 1(a)]. We assume that the vacuum–metal interface has a randomly rough structure, and the metal is characterized by a complex dielectric function $\varepsilon_2(\omega)$. The vacuum dielectric constant is $\varepsilon_1 \equiv 1$. The height of the surface is given by the single-valued function $x_3 = \zeta(\mathbf{x}_\parallel)$, where $\mathbf{x}_\parallel = (x_1, x_2, 0)$ is the lateral component of the position vector, $\mathbf{x}$. We assume that $\zeta(\mathbf{x}_\parallel)$ is at least once differentiable with respect to x_1 and x_2. The angles of incidence (θ_0, ϕ_0) and scattering (θ_s, ϕ_s) are defined positive according to the convention given in Fig. 1(b).

In this paper, we will consider randomly rough surfaces where $\zeta(\mathbf{x}_\parallel)$ constitutes a stationary random process defined by

$$\langle \zeta(\mathbf{x}_\parallel) \rangle = 0, \tag{1a}$$

$$\langle \zeta(\mathbf{x}_\parallel)\zeta(\mathbf{x}'_\parallel) \rangle = \delta^2 W(\mathbf{x}_\parallel - \mathbf{x}'_\parallel), \tag{1b}$$

where the angle brackets denote an average over an ensemble of surface realizations. In writing Eq. (1) we have defined the rms height of the surface, $\delta = \langle \zeta^2(\mathbf{x}_\parallel) \rangle^{1/2}$, and $W(\mathbf{x}_\parallel - \mathbf{x}'_\parallel)$ denotes the height–height autocorrelation function of the surface, normalized so that $W(\mathbf{0}) = 1$ [12] . In the discussion below, and when generating realizations of the surface profile function, it is more convenient to work with the power spectrum of the surface rather than using the autocorrelation function directly. The power spectrum, $g(\mathbf{k}_\parallel)$, of the surface profile function is defined by

$$g(\mathbf{k}_\parallel) = \int \mathrm{d}^2 x_\parallel W(\mathbf{x}_\parallel) \exp(-i\mathbf{k}_\parallel \cdot \mathbf{x}_\parallel), \tag{2}$$

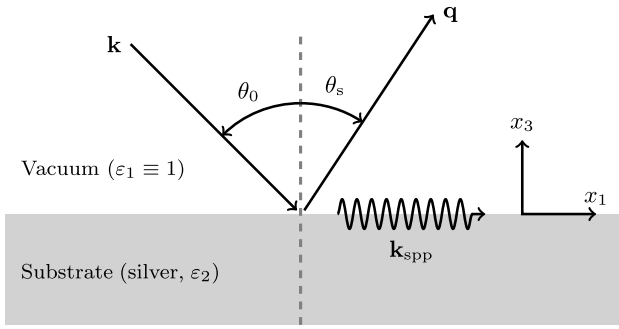

(a) System sketch, seen in the x_1x_3 plane.

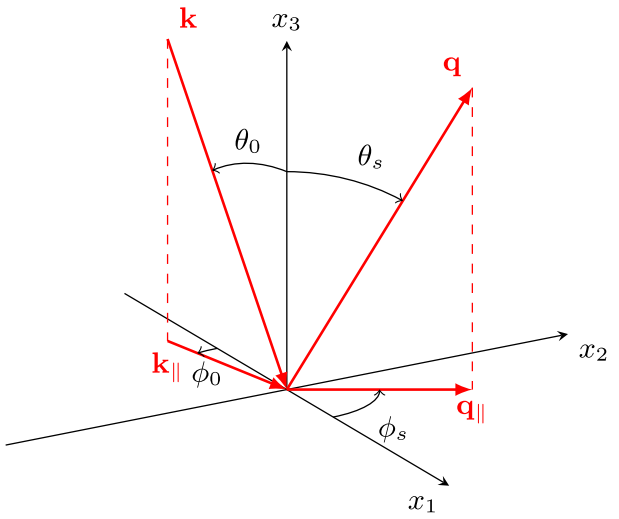

(b) Definition of wave vectors and polar angles.

Fig. 1. Sketches of the system under study (surface roughness not shown). (a) The light of wave vector $\mathbf{k}$ incident on the surface causes scattering into various propagating modes (of wave vector $\mathbf{q}$) and the excitation of SPPs ($\mathbf{k}_{spp}$). In this study, we assume $\varepsilon_1(\omega) \equiv 1$, and $\varepsilon_2(\omega)$ is taken from [11]. (b) Definition of the lateral wave vectors ($\mathbf{k}_\parallel$ and $\mathbf{q}_\parallel$) as well as the polar angles of incidence and scattering.

where $\mathbf{k}_\parallel = (k_1, k_2, 0)$ is the lateral component of the wave vector, $\mathbf{k}$. The power spectra that will be considered in this work are of the cylindrical form, where

$$g(k_\parallel) = \gamma_1 g_1(k_\parallel) + \gamma_2 g_2(k_\parallel) \tag{3a}$$

and g_i $(i = 1, 2)$ are given by [13]

$$g_i(k_\parallel) = \frac{4\pi}{k_+^2 - k_-^2} \theta(k_\parallel - k_-^{(i)}) \theta(k_+^{(i)} - k_\parallel). \tag{3b}$$

In Eq. (3a), γ_1 and γ_2 are real constants defined such that γ_1, $\gamma_2 \geq 0$ and $\gamma_1 + \gamma_2 = 1$. Furthermore, $k_\parallel = |\mathbf{k}_\parallel|$, $\theta(\cdot)$ denotes the Heaviside unit step function, and $k_\pm^{(i)}$ are wavenumber cutoff parameters, with $k_-^{(1)} < k_+^{(1)} < k_-^{(2)} < k_+^{(2)}$. The Heaviside step functions in Eq. (3b) cause each g_i to have a cylindrical shape: g_i is zero for $k_\parallel < k_-^{(i)}$, a positive constant for $k_-^{(i)} \leq k_\parallel < k_+^{(i)}$, and zero for $k_\parallel \geq k_+^{(i)}$. The constants γ_i determine the relative amplitudes of the outer and inner cylindrical parts of the power spectrum. The power spectrum described by Eq. (3) is a two-dimensional generalization of the one used by O'Donnell and Mendéz [9] and Simonsen [10] in their previous

numerical investigations of enhanced forward scattering from one-dimensional randomly rough surfaces.

We note that the power spectrum used by West and O'Donnell [6] in their experimental confirmation of enhanced backscattering is a one-dimensional special case of Eq. (3), with $\gamma_1 = 1$ and $\gamma_2 = 0$ (or vice versa).

A. Reduced Rayleigh Equation

The electric field in the vacuum above the surface [$x_3 > \max \zeta(\mathbf{x}_\parallel)$] can be expressed as the sum of an incident field and a scattered field,

$$\mathbf{E}(\mathbf{x}|t) = \left[\mathbf{E}^{(0)}(\mathbf{x}|\omega) + \mathbf{E}^{(s)}(\mathbf{x}|\omega)\right]\exp(-i\omega t), \tag{4}$$

where ω is the angular frequency of the incident (and scattered) light. The superscripts (0) and (s) on the electric field vectors indicate the incident and scattered field, respectively. Furthermore,

$$\mathbf{E}^{(0)}(\mathbf{x}|\omega) = \Big\{-\frac{c}{\omega}\left[\hat{\mathbf{k}}_\parallel \alpha_1(k_\parallel) + \hat{\mathbf{x}}_3 k_\parallel\right]\mathcal{E}_p^{(0)}(\mathbf{k}_\parallel) + (\hat{\mathbf{x}}_3 \times \hat{\mathbf{k}}_\parallel)\mathcal{E}_s^{(0)}(\mathbf{k}_\parallel)\Big\}\exp\left[i\mathbf{k}_\parallel \cdot \mathbf{x}_\parallel - i\alpha_1(k_\parallel)x_3\right], \tag{5a}$$

$$\mathbf{E}^{(s)}(\mathbf{x}|\omega) = \int \frac{\mathrm{d}^2 q_\parallel}{(2\pi)^2}\left\{\frac{c}{\omega}\left[\hat{\mathbf{q}}_\parallel \alpha_1(q_\parallel) - \hat{\mathbf{x}}_3 q_\parallel\right]\mathcal{E}_p^{(s)}(\mathbf{q}_\parallel) + (\hat{\mathbf{x}}_3 \times \hat{\mathbf{q}}_\parallel)\mathcal{E}_s^{(s)}(\mathbf{q}_\parallel)\right\}\exp\left[i\mathbf{q}_\parallel \cdot \mathbf{x}_\parallel + i\alpha_1(q_\parallel)x_3\right], \tag{5b}$$

where $\mathcal{E}_\alpha^{(0)}(\mathbf{q}_\parallel)$ and $\mathcal{E}_\beta^{(s)}(\mathbf{k}_\parallel)$, with $\alpha, \beta = p, s$ are the amplitudes of the α-polarized and β-polarized components of these fields with respect to the local planes of incidence and scattering, respectively. The wave vector of the incident light is $\mathbf{k}$, which is of length $|\mathbf{k}| = \omega/c$, where c is the speed of light in vacuum. The expressions in front of the field amplitudes are the unit polarization vectors. The wave vector of the scattered light, $\mathbf{q}$, has lateral component $\mathbf{q}_\parallel = (q_1, q_2, 0)$ and is related to the angles of scattering as indicated by Fig. 1(b). A caret over a vector indicates that it is a unit vector. Finally, the functions $\alpha_i(q_\parallel)$, $i = 1, 2$ are defined by

$$\alpha_i(q_\parallel) = \left[\varepsilon_i\left(\frac{\omega}{c}\right)^2 - q_\parallel^2\right]^{1/2}, \quad \times \operatorname{Re}\alpha_i(q_\parallel) > 0, \qquad \operatorname{Im}\alpha_i(q_\parallel) > 0. \tag{6}$$

A linear relation is assumed to exist between the amplitudes $\mathcal{E}_\alpha^{(s)}(\mathbf{q}_\parallel)$ and $\mathcal{E}_\beta^{(0)}(\mathbf{k}_\parallel)$ ($\alpha, \beta = p, s$), which we express in terms of the scattering amplitudes $R_{\alpha\beta}(\mathbf{q}_\parallel|\mathbf{k}_\parallel)$ [14]:

$$\mathcal{E}_\alpha^{(s)}(\mathbf{q}_\parallel) = \sum_{\beta=p,s} R_{\alpha\beta}(\mathbf{q}_\parallel|\mathbf{k}_\parallel)\mathcal{E}_\beta^{(0)}(\mathbf{k}_\parallel).$$

In order to obtain an equation for the scattering amplitudes, we first write down an expression for the transmitted field, $\mathbf{E}^{(t)}(\mathbf{x}|\omega)$, which is valid in the region $x_3 < \min \zeta(\mathbf{x}_\parallel)$ below the surface. We then assume the Rayleigh hypothesis, which states that for a sufficiently smooth surface, $|\nabla\zeta(\mathbf{x}_\parallel)| \ll 1$, these asymptotic expressions for the fields are valid also in the surface roughness region [$\min \zeta(\mathbf{x}_\parallel) < x_3 < \max \zeta(\mathbf{x}_\parallel)$] [15,16] and can be used to fulfill the boundary conditions satisfied by the electric and magnetic fields at the surface $x_3 = \zeta(\mathbf{x}_\parallel)$. From the resulting set of coupled matrix integral equations, it is possible to eliminate the amplitudes of the transmitted (reflected) field so that a single matrix integral equation results for the amplitudes corresponding to the field above (below) the surface. The resulting equation is known as the reduced Rayleigh equation for reflection (transmission). For details regarding the derivation of the reduced Rayleigh equation, we refer to [13] and [17].

If the scattering amplitudes are organized as the 2×2 matrix

$$\mathbf{R}(\mathbf{q}_\parallel|\mathbf{k}_\parallel) = \begin{pmatrix} R_{pp}(\mathbf{q}_\parallel|\mathbf{k}_\parallel) & R_{ps}(\mathbf{q}_\parallel|\mathbf{k}_\parallel) \\ R_{sp}(\mathbf{q}_\parallel|\mathbf{k}_\parallel) & R_{ss}(\mathbf{q}_\parallel|\mathbf{k}_\parallel) \end{pmatrix}, \tag{7}$$

the reduced Rayleigh equation for reflection from a two-dimensional surface can be written in the form [13,17,18]

$$\int \frac{\mathrm{d}^2 q_\parallel}{(2\pi)^2}\frac{I(\alpha_2(p_\parallel) - \alpha_1(q_\parallel)|\mathbf{p}_\parallel - \mathbf{q}_\parallel)}{\alpha_2(p_\parallel) - \alpha_1(q_\parallel)}\mathbf{M}^+(\mathbf{p}_\parallel|\mathbf{q}_\parallel)\mathbf{R}(\mathbf{q}_\parallel|\mathbf{k}_\parallel) = -\frac{I(\alpha_2(p_\parallel) + \alpha_1(k_\parallel)|\mathbf{p}_\parallel - \mathbf{k}_\parallel)}{\alpha_2(p_\parallel) + \alpha_1(k_\parallel)}\mathbf{M}^-(\mathbf{p}_\parallel|\mathbf{k}_\parallel), \tag{8a}$$

where

$$I(\gamma|\mathbf{Q}_\parallel) = \int \mathrm{d}^2 x_\parallel \exp[-i\gamma\zeta(\mathbf{x}_\parallel)]\exp(-i\mathbf{Q}_\parallel \cdot \mathbf{x}_\parallel), \tag{8b}$$

and

$$\mathbf{M}^\pm(\mathbf{p}_\parallel|\mathbf{q}_\parallel) = \begin{pmatrix} p_\parallel q_\parallel \pm \alpha_2(p_\parallel)\hat{\mathbf{p}}_\parallel \cdot \hat{\mathbf{q}}_\parallel \alpha_1(q_\parallel) & -\frac{\omega}{c}\alpha_2(p_\parallel)[\hat{\mathbf{p}}_\parallel \times \hat{\mathbf{q}}_\parallel]_3 \\ \pm\frac{\omega}{c}[\hat{\mathbf{p}}_\parallel \times \hat{\mathbf{q}}_\parallel]_3 \alpha_1(q_\parallel) & \frac{\omega^2}{c^2}\hat{\mathbf{p}}_\parallel \cdot \hat{\mathbf{q}}_\parallel \end{pmatrix}. \tag{8c}$$

The integral in Eq. (8b) is evaluated by expanding the exponential $\exp[-i\gamma\zeta(\mathbf{x}_\parallel)]$ in powers of its argument and integrating the resulting series term by term by the fast Fourier transform. In practice, the sum is truncated at a finite order sufficient to give convergent results ($n = 20$ was used in this work). The integration domain used for the integral in Eq. (8a) is truncated to cover the circular region $q_\parallel \leq Q/2$, and the integration was converted to a finite sum over this domain by a two-dimensional version of the standard midpoint quadrature scheme. From this sum, we can obtain a linear system of equations (one for each value of $\mathbf{p}_\parallel$), which can be solved to find $R_{\alpha\beta}(\mathbf{q}_\parallel|\mathbf{k}_\parallel)$.

For the simulations presented in this paper, we have used numerically generated, discrete realizations of the surface profile function. These realizations covered a square area of size $L \times L$ in the x_1x_2 plane, determining the integration limits in Eq. (8b). The surface realizations were discretized onto a quadratic, equidistant grid of $N_x \times N_x$ points. Each realization was generated by a two-dimensional version of the Fourier filtering method presented in, for instance, [19,20]. For a detailed discussion of how one can proceed to solve the reduced Rayleigh equation numerically, we refer to [21].

B. Mean Differential Reflection Coefficient

When the incident field is known, the quantity $R_{\alpha\beta}(\mathbf{q}_\parallel|\mathbf{k}_\parallel)$ completely specifies the total electromagnetic field in the region $x_3 > \max \zeta(\mathbf{x}_\parallel)$. However, $R_{\alpha\beta}(\mathbf{q}_\parallel|\mathbf{k}_\parallel)$ is not directly measurable in experiments. A quantity well suited for experimental studies is the mean differential reflection coefficient (MDRC), $\langle \partial R_{\alpha\beta}/\partial\Omega_s \rangle$, which is defined as the time-averaged fraction of the incident power scattered into the solid angle $\mathrm{d}\Omega_s$ about the scattering direction, $\hat{\mathbf{q}}$. The relationship between $R_{\alpha\beta}(\mathbf{q}_\parallel|\mathbf{k}_\parallel)$ and the MDRC can be written as [13]

$$\left\langle \frac{\partial R_{\alpha\beta}}{\partial \Omega_s} \right\rangle = \frac{1}{L^2}\frac{\omega^2}{4\pi^2 c^2}\frac{\cos^2\theta_s}{\cos\theta_0}\langle |R_{\alpha\beta}(\mathbf{q}_\parallel|\mathbf{k}_\parallel)|^2\rangle. \tag{9}$$

Because we are studying weakly rough surfaces, light scattered coherently (specularly) by the rough surface will dominate. However, some of the light incident on the surface will also be scattered incoherently (diffusely) by the rough surface. In theoretical and numerical studies, it is advantageous to separate these two contributions.

By light scattered coherently by the surface, we mean scattered light that is in phase from one surface realization to the next, so that the intensity of light scattered coherently (from β to α polarization) will be proportional to $|\langle R_{\alpha\beta}(\mathbf{q}_\parallel|\mathbf{k}_\parallel)\rangle|^2$. The contribution to the MDRC from the light that has been scattered *incoherently* by the rough surface is defined as [13]

$$\left\langle \frac{\partial R_{\alpha\beta}}{\partial \Omega_s} \right\rangle_{\mathrm{incoh}} = \frac{1}{L^2}\frac{\omega^2}{4\pi^2 c^2}\frac{\cos^2\theta_s}{\cos\theta_0} \times \left[\langle |R_{\alpha\beta}(\mathbf{q}_\parallel|\mathbf{k}_\parallel)|^2\rangle - |\langle R_{\alpha\beta}(\mathbf{q}_\parallel|\mathbf{k}_\parallel)\rangle|^2\right]. \tag{10}$$

The contribution to the MDRC from the light scattered *coherently* is therefore given by the difference between Eqs. (9) and (10). We will see below that enhanced backscattering and enhanced forward scattering are both phenomena observed in the *incoherent component* of the MDRC, even if in the case of enhanced forward scattering it is observed in the *specular direction*.

We also note that the quantity $R_{\alpha\beta}(\mathbf{q}_\parallel|\mathbf{k}_\parallel)$ can be used to construct the Mueller matrix for reflection from a rough surface [22]. The Mueller matrix contains all linear transformations of the polarization of light undergoing scattering from a rough surface, including polarization and depolarization.

C. SPPs

SPPs are electromagnetic modes that are confined to dielectric–metal interfaces, where the dielectric function of the cladding is positive and the (real part of the) dielectric function of the substrate is smaller than the negative of the dielectric function of the cladding [23]. The dispersion relation of SPPs at a flat vacuum–metal interface is [23]

$$k_{\mathrm{spp}}(\omega) = \frac{\omega}{c}\left(\frac{\varepsilon_2(\omega)}{\varepsilon_2(\omega)+1}\right)^{1/2}, \tag{11}$$

where $k_{\mathrm{spp}}(\omega)$ is the length of the wave vector of the SPP mode. For silver at wavelength $\lambda = 457.9$ nm (in vacuum), for which the dielectric function is $\varepsilon_2(\omega) = -7.5 + 0.24i$ [11], it follows that $k_{\mathrm{spp}} = (1.074 + 0.003i)\omega/c$ $(\omega = 2\pi c/\lambda)$. The imaginary part of k_{spp} can be interpreted as an inverse decay length of the SPP mode, whereas the real part corresponds to the wave number of the mode.

Multiple scattering phenomena such as the enhanced backscattering and enhanced forward scattering are, for weakly rough surfaces, typically caused by the incident light exciting SPPs that are subsequently scattered zero or more times before coupling into a mode propagating away from the surface [12]. In particular, in one-dimensional small-amplitude perturbation theory, the lowest-order contribution to the enhanced forward scattering peak in the MDRC has its origin in quadruple scattering processes [7, Fig. 10].

D. Allowed and Forbidden Scattering Processes

From small-amplitude perturbation theory [12,24], it can be shown that a *single* scattering event from lateral wave vector $\mathbf{k}_\parallel$ to $\mathbf{q}_\parallel$ is allowed only if the power spectrum evaluated at the wave vector transfer $\mathbf{k}_{\mathrm{sc}}$ is nonzero, that is,

$$g(\mathbf{k}_{\mathrm{sc}}) > 0, \qquad \mathbf{k}_{\mathrm{sc}} = \mathbf{q}_\parallel - \mathbf{k}_\parallel. \tag{12}$$

This condition holds for scattering between propagating modes; between evanescent modes; and from propagating to evanescent modes and vice versa. For isotropic power spectra, such as those studied in this paper [Eq. (3)], the requirement of Eq. (12) simplifies to

$$g(|\mathbf{k}_{\mathrm{sc}}|) > 0. \tag{13}$$

To better understand the physical implications of the condition in Eq. (13), and to facilitate our interpretation of the simulation results presented later in this paper, we present a visual model for discussing relevant scattering processes in Fig. 2. Before starting the discussion, we remind the reader that modes for which $k_\parallel \le \omega/c$ are propagating in the vacuum, whereas for $k_\parallel > \omega/c$ the corresponding fields are evanescent, that is, the field amplitudes decay exponentially along both directions perpendicular to the surface. Moreover, at the wavelength $\lambda = 457.9$ nm, assumed in the simulations presented below, the vacuum–silver interface supports SPPs of lateral wave vector $k_{\mathrm{spp}} = 1.074\omega/c$ (see Section 2.C). For simplicity, we have neglected the imaginary part of the wavenumber, as it is small compared to its real part.

In passing, we note that the polarization state of light can be modified at each scattering event, subject to the requirement that SPPs are always p-polarized. We will, however, not discuss polarization effects of single scattering events in this section.

We will now discuss Fig. 2, which was produced under the assumption that the surface power spectrum is identical to that in Eq. (3) and characterized by the values for $k_\pm^{(i)}$ used in the later simulations (Section 3): $k_-^{(1)} = 0.782\omega/c$, $k_+^{(1)} = 1.366\omega/c$, $k_-^{(2)} = 2.048\omega/c$, and $k_+^{(2)} = 2.248\omega/c$. The annular regions, indicated by blue shaded regions in Fig. 2, represent the nonzero parts of the surface roughness power spectrum.

First, we consider the scattering process $\mathbf{k}_\parallel \to \mathbf{q}_\parallel$ [Fig. 2(a)] that corresponds to the lateral wave vector (or momentum) transfer $\mathbf{k}_{\mathrm{sc}}$. In Fig. 2(a) the incident lateral wave vector, $\mathbf{k}_\parallel$, is placed so that it starts at the origin of wave vector space, O; the same is done for $\mathbf{q}_\parallel$. We superpose blue shaded regions representing the power spectrum so that the center of the

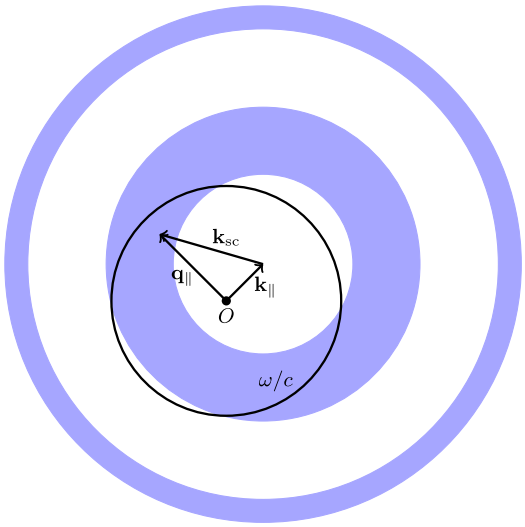

(a) Scattering from wave vector $\mathbf{k}_{\|}$ into wave vector $\mathbf{q}_{\|}$. The scattered mode is propagating, since $|\mathbf{q}_{\|}| < \omega/c$, with ω/c indicated by the black ring.

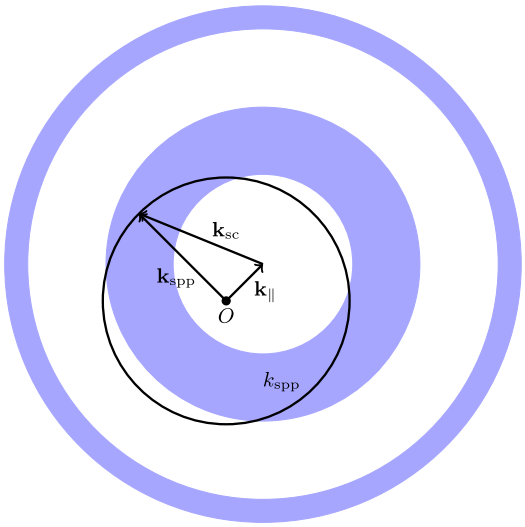

(b) Excitation of a surface plasmon polariton by incident light. The surface plasmon polariton is not propagating in vacuum, as $k_{spp} > \omega/c$. The parts of the black ring (of radius k_{spp}) which lie in the blue region represent legal SPP excitation processes.

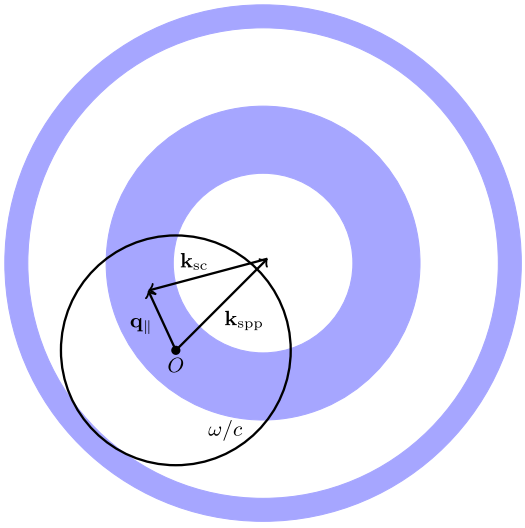

(c) Scattering of a surface plasmon polariton into a bulk propagating mode. Legal propagating modes are those for which $\mathbf{q}_{\|}$ lies inside the blue region and $q_{\|} < \omega/c$.

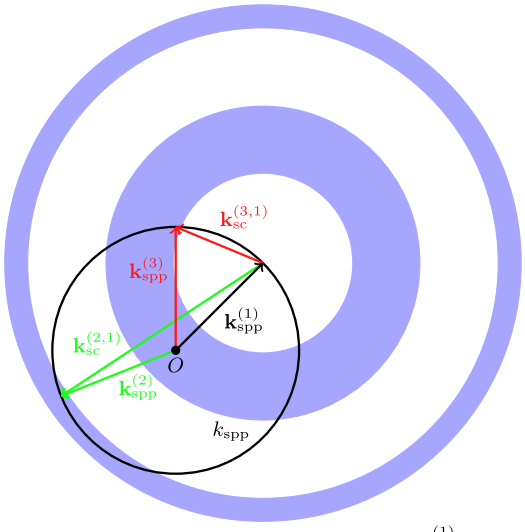

(d) Scattering of a surface plasmon polariton ($\mathbf{k}_{spp}^{(1)}$). Two legal scattered modes ($\mathbf{k}_{spp}^{(2)}$ and $\mathbf{k}_{spp}^{(3)}$) are shown. The black ring indicates legal wave vectors for SPPs.

Fig. 2. Four scattering processes important for understanding the results of this study. A detailed discussion of the figure is found in the text. All subfigures (a)–(d) are drawn to correct and identical scale for the parameters $k_{\pm}^{(i)}$ and ε_2 used throughout this study. The blue annular regions indicate the nonzero parts of the power spectrum, that is, the ranges of $\mathbf{k}_{sc}$ allowed by the power spectrum. The lengths of $\mathbf{k}_{\|}$ in (a) and (b) correspond to $(\theta_0, \phi_0) = (27°, 45°)$.

power spectrum is located at the end of $\mathbf{k}_{\|}$. Thus, if $\mathbf{k}_{sc}$ indicates a point inside the blue shaded regions (the power spectrum), the scattering process $\mathbf{k}_{\|} \to \mathbf{q}_{\|}$ is allowed. Moreover, at the same time, if $q_{\|} \leq \omega/c$, the process $\mathbf{k}_{\|} \to \mathbf{q}_{\|}$ results in a scattered mode that can propagate away from the surface. On the assumption that both $\mathbf{k}_{\|}$ and $\mathbf{q}_{\|}$ are propagating in vacuum, one realizes that $\mathbf{k}_{\|}$ [for the value of $\mathbf{k}_{\|}$ used in Fig. 2(a)] can be converted into $\mathbf{q}_{\|}$ through a single interaction with the surface roughness (single scattering) only within a *crescent-like* region. This region is defined by the shaded blue region that resides inside the circle $q_{\|} = \omega/c$, indicated in black in Fig. 2(a). Outside this crescent region, the scattering process is either not allowed or $q_{\|} > \omega/c$, meaning that the mode is evanescent (nonpropagating). When later studying the full angular distribution of the scattered light (Fig. 3), we will see that this observation is important.

We now turn to the possibility of exciting SPPs by the incident light, a situation addressed in Fig. 2(b). The excitation $\mathbf{k}_{\|} \to \mathbf{k}_{spp}$ of SPPs is subject to the constraints in Eq. (13). In particular, we have that the excitation of an SPP by the incident field characterized by $\mathbf{k}_{\|}$ is only allowed if

$$k_{-}^{(1)} < |\mathbf{k}_{spp} - \mathbf{k}_{\|}| < k_{+}^{(1)}, \tag{14}$$

or (less relevant for the parameters used in this study, due to the large θ_0 required)

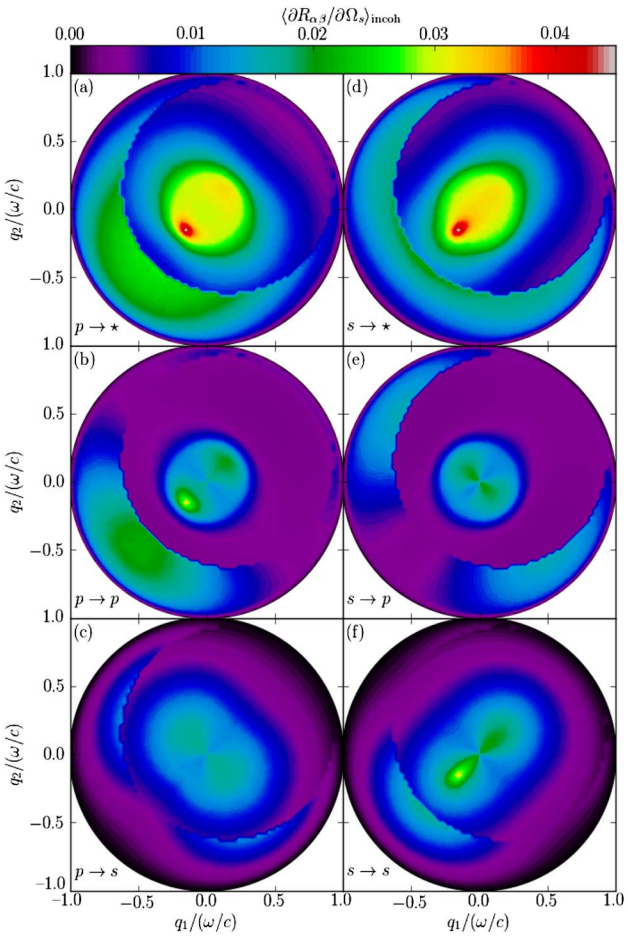

Fig. 3. Full angular distribution of the incoherent contribution to the MDRC, assuming the surface properties stated in the text. The angles of incidence were $(\theta_0, \phi_0) = (12.5°, 45°)$. The subplots show scattering (b) from p polarization to p polarization, (e) $s \to p$, (c) $p \to s$, and (f) $s \to s$. In (a), the incident light was p-polarized, but the polarization of the scattered light was not recorded, and in (d) the incident light was s-polarized. The enhanced forward scattering peak is most easily seen in the $p \to p$ configuration (b). The sharp circular edge, centered on $\mathbf{k}_\parallel$, is caused by the suppression of single scattering due to the form of the power spectrum; see discussion in Section 2.D, Eq. (3), and Fig. 2(a).

$$k_-^{(2)} < |\mathbf{k}_{\text{spp}} - \mathbf{k}_\parallel| < k_+^{(2)}. \tag{15}$$

Consequently, it is only possible (for the power spectrum used in this study) to excite SPPs for small (or very large) angles of incidence. The excitation of an SPP is shown in Fig. 2(b). The black ring indicates the length of the possible SPP wave vectors. In the plane of incidence, SPPs cannot be excited by the incident light for angles of incidence $\theta_0 > 17°$. For out-of-plane scattering, however, SPP excitation is allowed also for $\theta_0 > 17°$. This is qualitatively different from scattering from a one-dimensionally rough surface.

E. Enhanced Backscattering

For weakly rough surfaces, the presence of the enhanced backscattering phenomenon typically requires the excitation of SPPs. For strongly rough surfaces, on the other hand, it can take place through multiple scattering between vacuum-propagating modes [25,26]. For the weakly rough surfaces discussed here, the SPP channel is by far the dominant contribution to the backscattering enhancement. As such, the presence of the enhanced backscattering phenomenon for weakly rough surfaces requires first that incident light can couple to SPPs, that is, $g(|\mathbf{k}_{\text{spp}} - \mathbf{k}_\parallel|) > 0$, as discussed in the previous paragraph. Second, the existence of enhanced backscattering requires that SPPs can couple out into the antispecular direction, that is, that $g(|-\mathbf{k}_\parallel - \mathbf{k}_{\text{spp}}|) > 0$. This implies, with the power spectrum used here, that

$$k_-^{(1)} < |\mathbf{k}_{\text{spp}} + \mathbf{k}_\parallel| < k_+^{(1)}. \tag{16}$$

Coupling from SPPs to vacuum-propagating modes is illustrated in Fig. 2(c). For the parameters used in this study, the outer cylindrical part of the power spectrum essentially does not contribute to the scattering process $\mathbf{k}_{\text{spp}} \to \mathbf{k}_\parallel$, as $k_-^{(2)} \approx \omega/c + k_{\text{spp}}$.

For one-dimensionally randomly rough surfaces [7,10], the scattered wave vectors are confined to the plane of incidence, and all quantities in Eqs. (12)–(16) can be written as scalars. Thus, there is a sharp and well-defined angular cutoff for the excitation of SPPs in this case. For two-dimensionally rough surfaces, however, incident light can couple to SPPs that do not propagate in the plane of incidence. This can allow scattering processes that would be forbidden in the one-dimensional case, and any limits derived using the one-dimensional model will become "fuzzy" for two-dimensional surfaces.

F. Enhanced Forward Scattering

For SPPs to contribute to enhanced forward scattering, it is required that the power spectrum allows both the excitation and counterpropagation of SPPs, as well as coupling from SPPs to vacuum-propagating modes in the specular direction.

For the scattering of an SPP of wavevector $\mathbf{k}_{\text{spp}}^{(1)}$ to an SPP of wavevector $\mathbf{k}_{\text{spp}}^{(2)}$ to be allowed, it is required that $g(|\mathbf{k}_{\text{spp}}^{(2)} - \mathbf{k}_{\text{spp}}^{(1)}|) > 0$. For the power spectrum used in this study, this condition is fulfilled if

$$k_-^{(1)} < |\mathbf{k}_{\text{spp}}^{(2)} - \mathbf{k}_{\text{spp}}^{(1)}| < k_+^{(1)} \tag{17}$$

or

$$k_-^{(2)} < |\mathbf{k}_{\text{spp}}^{(2)} - \mathbf{k}_{\text{spp}}^{(1)}| < k_+^{(2)}. \tag{18}$$

The counterpropagation requirement is the rationale for adding the outer annulus to the power spectrum of Eq. (3). This annulus is narrow and centered at $k_\parallel = 2k_{\text{spp}}$, meaning that it facilitates scattering where $|\mathbf{k}_{\text{sc}}| \approx 2k_{\text{spp}}$, that is, counterpropagation of SPPs. This corresponds to the fulfillment of Eq. (18) and is illustrated by the green vectors in Fig. 2(d) ($\mathbf{k}_{\text{spp}}^{(2)}$ and $\mathbf{k}_{\text{spp}}^{(2,1)}$).

We note that for two-dimensionally rough surfaces it is possible for an SPP to be scattered out of plane by the g_1 part of the power spectrum. This can happen when Eq. (17) is fulfilled, as shown in red in Fig. 2(d), where the resulting lateral wave vector is denoted $\mathbf{k}_{\text{spp}}^{(3)}$.

The principles discussed above are also valid for systems consisting of a metallic substrate on which a dielectric thin film has been deposited, with a vacuum or lossless dielectric cladding, where either interface of the film is randomly rough [27]. The generalization to different power spectra should also

be obvious. We note that if the power spectrum of the randomly rough surface is, for example, Gaussian, the single scattering contribution to the MDRC is typically dominant. In such cases, it can be challenging to separate single scattering effects from multiple scattering effects.

3. RESULTS

In this section, we present results for the MDRC when light is scattered from rough silver surfaces. For all the results presented here, the (vacuum) wavelength of the incident light was $\lambda = 457.9$ nm, and the dielectric function of the Ag substrate at this wavelength is $\varepsilon_2 = -7.5 + 0.24i$. The vacuum dielectric function is $\varepsilon_1 = 1$. The rough surfaces were characterized by the power spectrum of Eq. (3), defined by the wavenumber parameters $k_-^{(1)} = 0.782\omega/c$, $k_+^{(1)} = 1.366\omega/c$, $k_-^{(2)} = 2.048\omega/c$, and $k_+^{(2)} = 2.248\omega/c$. Furthermore, the amplitudes γ_i were chosen such that $\gamma_2/\gamma_1 = 0.75$, which was found in [10] to give a relatively strong enhanced forward scattering effect. The rms surface roughness was taken to be $\delta = 0.025\lambda$; the edge of the square region covered by the rough surface was $L = 36\lambda$; and this region was discretized at a grid of $N_x = 359$ points along each of the x_1 and x_2 directions.

As the Nyquist theorem [28] relates resolution in position space and wave vector space, the values of N_x and L lead to the following numerical parameters: the wavenumber cutoff in the integral in Eq. (8a) was $\mathcal{Q}/2 = 2.493\omega/c$; the resolution in $\mathbf{q}_\parallel$ was $\Delta q = 0.0279\omega/c$; and $N_q = 180$ values of $\mathbf{q}_\parallel$ were resolved along each of the q_1 and q_2 axes [21]. The results presented were obtained by averaging the results over an ensemble of 10,825 surface realizations. Simulating the scattering from one surface realization took approximately 17 min on a machine with two six-core AMD Opteron 2.4 GHz processors and required about 12 GB of memory. For a discussion of the details of how the calculations were performed, we refer to [21].

In Fig. 3, we present the full angular distribution of the MDRC, including polarization effects. Figures 3(a)–3(c) show the MDRC for p-polarized incident light, and in Figs. 3(d)–3(f) the incident light was s-polarized. In the upper row, the polarization of the scattered light was not recorded; in the second row, only the p-polarized component of the scattered light was recorded; and in the third row, only the s-polarized component of the scattered light was recorded. The full angular intensity distribution displays important information hidden from the reader of in-plane or out-of-plane cuts of the MDRC (e.g., Fig. 4). Notably, we observe that the intensity distribution depends on which linear polarization is used to illuminate the surface as well as which linear polarization is recorded in the (simulated) detector. Furthermore, the crescent regions of the MDRC of high intensity show for which angles of scattering single scattering is allowed, as per the theoretical discussion in Section 2.D.

One of the significant differences between the light scattering from one-dimensional and two-dimensional rough surfaces is the absence of polarization effects in the former case (assuming the plane of incidence to be perpendicular to the grooves of the surface). Notably, for light scattering from rough two-dimensional surfaces, the light scattered out-of-plane is significantly cross-polarized.

The enhanced forward scattering phenomenon expresses itself as a peak in the specular direction of the intensity of the light scattered incoherently by the rough surface. For this reason, in Figs. 4 and 5 we present the incoherent component of the MDRC in the plane of incidence (i.e., for $\phi_s = \phi_0$).

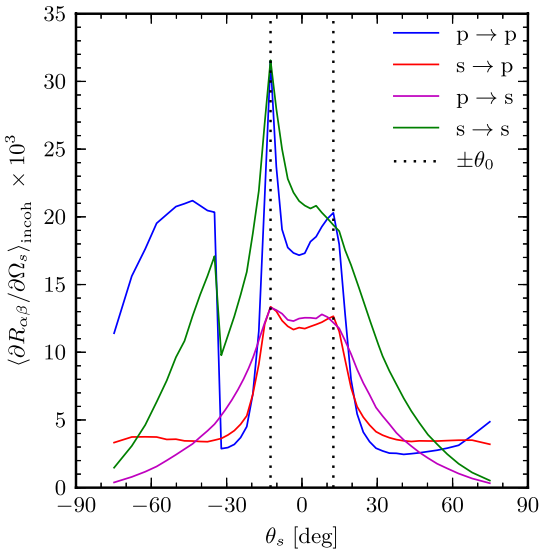

Fig. 4. In-plane (i.e., for $\phi_s = \phi_0$) part of the MDRC for light scattered from a rough silver surface with rms roughness $\delta = 0.025\lambda$. The angles of incidence were $(\theta_0, \phi_0) = (12.5°, 45°)$. The results were obtained by averaging over 10,825 surface realizations. The most prominent enhanced forward scattering peak is in $p \to p$ polarization, but a small contribution in $s \to p$ polarization can also be seen. Enhanced backscattering is observed in all polarization combinations.

Figure 4 shows the incoherent component of the MDRC for $\theta_0 = 12.5°$, for all combinations of incident and scattered polarizations. Because SPPs can only be excited in p polarization, it is reasonable to assume that light scattered through the temporary creation of an SPP will be predominantly p-polarized. When examining Fig. 4, we only observe enhanced

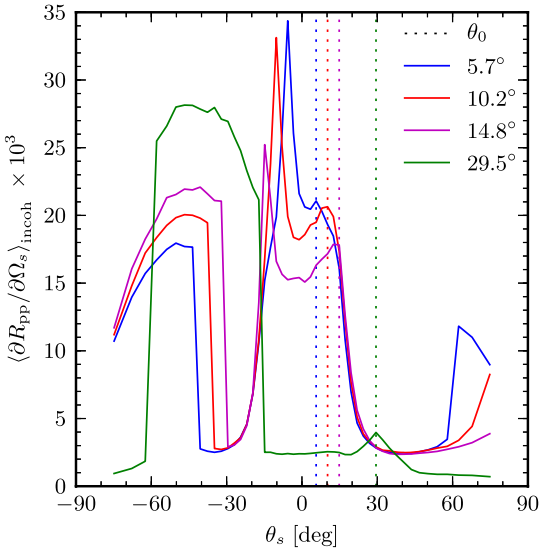

Fig. 5. $p \to p$ contribution to the MDRC for the same surface properties as in Fig. 4 for several different angles of incidence. In all cases, we observe the enhanced forward scattering peak. The effect is most powerful in the vicinity of $\theta_0 \approx 12°$. For polar angle of incidence $\theta_0 = 29.5°$, it is not possible to achieve enhanced forward scattering through the in-plane SPP channel; hence, the peak at $\theta_s = 29.5°$ has a different explanation.

forward scattering, that is, a peak in the forward direction, for $p \to p$ and $s \to p$ scattering. We also note that the enhanced forward scattering peak is much more well defined in $p \to p$ than in $s \to p$ scattering. It is worth noting that for angles $\theta_s > -34.4°$, in-plane single scattering of light is forbidden due to the power spectrum used [Eq. (3) and Fig. 2]. Consequently, the "edge" seen at the left-hand side of Fig. 4 is mainly caused by the single scattering of light for angles $\theta_s \leq -34.4°$.

By studying the θ_0 dependence of $\langle \partial R_{pp}/\partial\Omega_s \rangle$ (Fig. 5), several effects caused by the shape of the power spectrum can be observed. The positions of the "edges" caused by the suppression of single scattering are directly related to the power spectrum: to the leading order in the surface profile function, the intensity of single scattering is proportional to the power spectrum of the surface [12,24]. For the surface parameters assumed here, single scattering is forbidden for $|\mathbf{q}_\parallel - \mathbf{k}_\parallel| < k_-^{(1)} = 0.782\omega/c$. Thus, the cylindrical shape of the power spectrum leads to a region around $\mathbf{k}_\parallel$ into which less light is scattered, as single scattering is suppressed here.

Also in Fig. 5, a sharp edge is observed for the case of $\theta_0 = 29.5°$, at $\theta_s \approx -60°$. The location of this edge is given by the outer edge of the inner cylinder of the power spectrum, $k_+^{(1)}$. Due to the power spectrum vanishing between the inner and outer cylinder [Eq. (3)], single scattering is forbidden for $\theta_s < -60°$.

Of greater interest, and one of the main points of this paper, are the peaks observed in the forward and backward directions. The vertical dotted lines in Figs. 4 and 5 show the expected positions of the enhanced forward scattering peaks, and we see that in each case, these coincide with the observed peaks. The effect is most pronounced for the polar angle of incidence around $\theta_0 \approx 12°$. For angles of incidence above 17°, it is not possible for SPPs to be excited in the plane of incidence because the power spectrum in Eq. (3) is zero for $k_\parallel + k_{\mathrm{spp}} > k_+^{(1)}$ for in-plane scattering [10]. Nevertheless, a peak in the incoherent part of the MDRC and in the specular direction is visible for $\theta_0 = 29.5°$. Our interpretation is that the origin of this peak is the presence of the g_2 part of the power spectrum; see Fig. 7(b) and the corresponding discussion.

In accordance with previous work on light scattering from two-dimensionally randomly rough surfaces [17–19,21,22,27], we observe enhanced backscattering in Figs. 4 and 5. The enhanced backscattering peak is located in the retroreflection direction, $\theta_s = -\theta_0$. The effect is present in both copolarized and cross-polarized scattering. This is in contrast to the case of one-dimensional surface roughness, where enhanced backscattering can only be observed in the $p \to p$ polarization configuration.

A complete scan of the angles of incidence for which one observes enhanced backscattering and enhanced forward scattering is presented in Fig. 6. In these figures, the enhanced backscattering peak and the enhanced forward scattering peak are shown as "ridges" in the color map. As the ridges follow the $\pm\theta_s$ directions very well, we conclude that they indeed represent the phenomena of enhanced backscattering and enhanced forward scattering. For enhanced forward scattering, which is a quadruple scattering effect, the peak is somewhat broader than the enhanced backscattering peak, which is a double (or higher-order) scattering effect. Briefly put, the two-dimensional nature of the rough surface allows for more freedom in the choice of scattered wave vectors, leading to a wider peak.

For comparison with the results shown in Fig. 5, we have also performed simulations for the cases where $\gamma_1 = 1, \gamma_2 = 0$ [Fig. 7(a)], or where $\gamma_1 = 0$, $\gamma_2 = 1$ [Fig. 7(b)]. In the former case, only the inner annulus of the power spectrum is present, and in the latter case, only the outer annulus is present. The other simulation parameters were as follows. The edges of the simulation domain in the x_1x_2 plane was $L = 30\lambda$ and was discretized at $N_x = 319$ points along each of the lateral axes. The

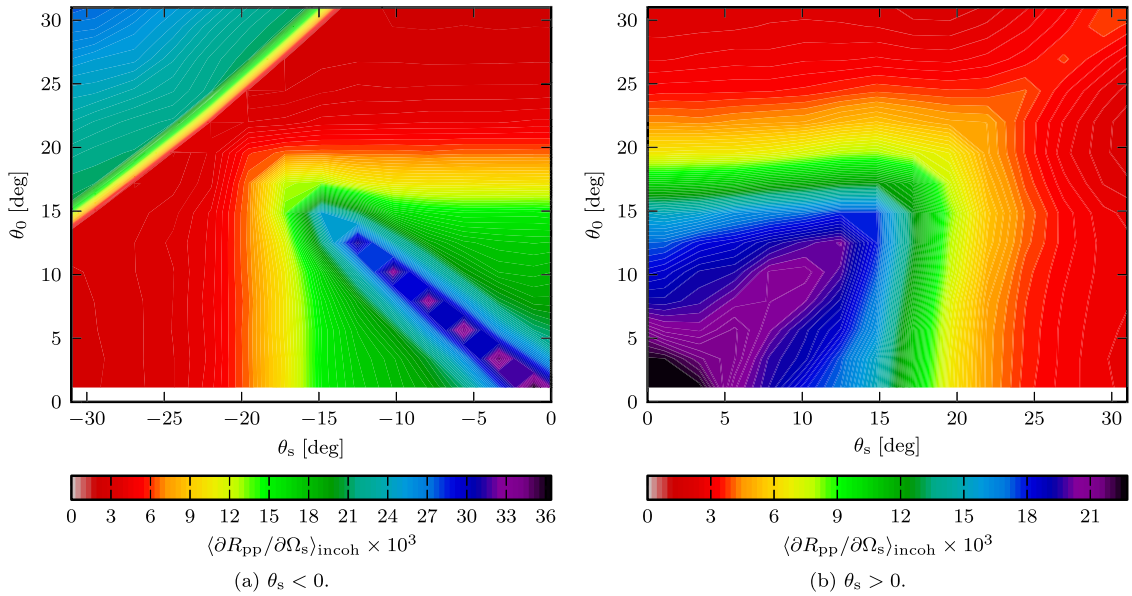

(a) $\theta_s < 0$. (b) $\theta_s > 0$.

Fig. 6. Contour plots of the incoherent, in-plane, and $p \to p$ part of the MDRC as a function of angle of incidence (θ_0) and scattering (θ_s). We assume $\phi_s = \phi_0$ in these figures. (a) The enhanced backscattering peak is shown as a purple "ridge" at $\theta_s = -\theta_0$. The oscillatory behavior with angle of incidence that the enhanced backscattering peak seems to exhibit in (a) is believed to be an artifact of the interpolation routine used to produce the figure from the discrete simulation data. (b) The enhanced forward scattering peak is shown as a purple "ridge" at $\theta_s = \theta_0$. Note that the color map has been truncated [cf. (a)] to show the peak more clearly.

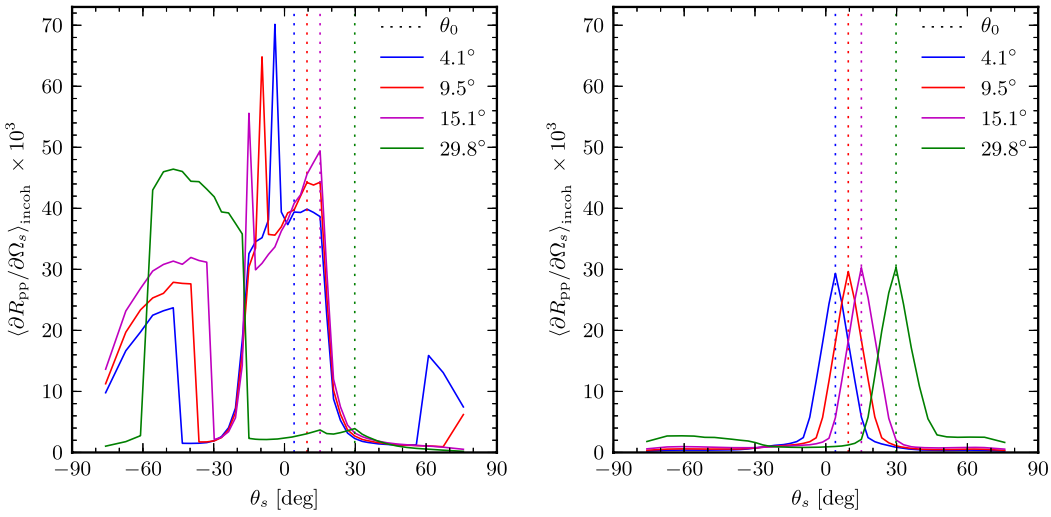

(a) In-plane part of the p → p contribution to the MDRC for a power spectrum with $\gamma_1 = 1$ and $\gamma_2 = 0$.

(b) In-plane part of the p → p contribution to the MDRC for power spectrum with $\gamma_1 = 0$ and $\gamma_2 = 1$.

Fig. 7. In-plane $p \to p$ scattering for power spectra with (a) $\gamma_1 = 1$, $\gamma_2 = 0$ and (b) $\gamma_1 = 0$, $\gamma_2 = 1$. With $\gamma_1 = 0$, $\gamma_2 = 1$, coupling into SPPs is suppressed. With $\gamma_1 = 1$, $\gamma_2 = 0$, coupling into SPPs is allowed but not scattering from an SPP to a counterpropagating SPP. This allows enhanced backscattering but not enhanced forward scattering.

dielectric function, the power spectrum parameters $k_{\pm}^{(i)}$, and the rms surface roughness parameters were the same as before. The parameters N_x and L were reduced for these simulations in order to save computer resources. This also leads to a different discrete set of θ_s being resolved (cf. Fig. 5).

The results for $\gamma_1 = 1$, $\gamma_2 = 0$ are presented in Fig. 7(a). In this case, incident light can couple to SPPs, but it is not possible to couple from one SPP to another SPP traveling in the opposite direction (counterpropagation). Thus, enhanced backscattering, which to the lowest order is a double scattering process, is allowed. Enhanced forward scattering, on the other hand, is a quadruple scattering process, dependent on scattering from SPPs to counterpropagating SPPs. Hence, there is no enhanced forward scattering peak when $\gamma_2 = 0$. The shoulder visible in Fig. 7(a) does not move as θ_0 increases, meaning that it is not related to the enhanced forward scattering phenomenon but is a result of the shape of the power spectrum.

In Fig. 7(b), we show the results for $\gamma_1 = 0$, $\gamma_2 = 1$. In this case, both single scattering and coupling from incident light to SPPs are prohibited. Instead, incident light will excite evanescent modes which are not resonant modes of the surface. These may be scattered several times before coupling out into vacuum-propagating modes. The width of the triangular structure seen in the MDRC in Fig. 7(b) is determined by the width of the outer annulus of the power spectrum.

In order to verify the correctness of the numerical results, the total reflected power normalized by the total incident power was calculated. In all cases it was found to be lower than 1, which is expected due to absorption. If one (artificially) assumes the substrate to be lossless, the normalized reflected power should in principle be identical to 1. For the surface parameters used in this study, and with $\mathrm{Im}(\varepsilon_2) = 0$, the normalized total reflected power was 1.000 ± 0.007 for all angles of incidence. We stress that the conservation of energy is a necessary, but not sufficient, criterion for the validity of the simulation results [21].

4. CONCLUSION

In conclusion, we have studied, by a nonperturbative numerical method, two phenomena observed in rough surface scattering, namely enhanced forward scattering and enhanced backscattering. These are both phenomena observed in the diffuse (incoherent) part of the MDRC and are caused by constructive interference between SPPs propagating along a vacuum–metal interface. In particular, the observation of enhanced forward scattering has not previously been reported for systems containing two-dimensionally rough surfaces. The two-dimensional nature of the rough surface studied here gives significantly more freedom in the allowed scattering channels when compared to one-dimensionally rough surfaces, giving less sharp “cutoffs” caused by the power spectrum.

A simple visual model for determining which scattering processes are allowed by two-dimensionally rough surfaces has also been given (Fig. 2). This model can be used to determine for which combinations of angles of incidence and scattering enhanced backscattering and enhanced forward scattering can be observed.

The enhanced forward and backward scattering phenomena are dependent on the presence of surface-guided modes. Enhanced backscattering has already been observed in a thin-film system in both polarizations [27]. We expect that enhanced forward scattering can also be observed in thin-film systems for all polarization combinations, as such structures support surface-guided modes in both p and s polarizations. We leave this investigation to future work, as the required computational effort is significant.

ACKNOWLEDGMENTS

The authors would like to thank Dr. A. A. Maradudin for fruitful interactions. The work of Tor Nordam was supported by the Nordic Center of Excellence in PV funded by Nordic Energy Research (contract no. 06-Renew-C31).

REFERENCES AND NOTE

1. E. Ozbay, "Plasmonics: merging photonics and electronics at nanoscale dimensions," Science **311**, 189–193 (2006).
2. H. A. Atwater and A. Polman, "Plasmonics for improved photovoltaic devices," Nat. Mater. **9**, 205–213 (2010).
3. A. Savchenko, E. Kashuba, V. Kashuba, and B. Snopok, "Imaging technique for the screening of protein–protein interactions using scattered light under surface plasmon resonance conditions," Anal. Chem. **79**, 1349–1355 (2007).
4. A. Savchenko, E. Kashuba, V. Kashuba, and B. Snopok, "Imaging of plasmid DNA microarrays by scattering light under surface plasmon resonance conditions," Sens. Lett. **6**, 705–713 (2008).
5. A. R. McGurn, A. A. Maradudin, and V. Celli, "Localization effects in the scattering of light from a randomly rough grating," Phys. Rev. B **31**, 4866–4871 (1985).
6. C. S. West and K. A. O'Donnell, "Observations of backscattering enhancement from polaritons on a rough metal surface," J. Opt. Soc. Am. A **12**, 390–397 (1995).
7. K. A. O'Donnell, "High-order perturbation theory for light scattering from a rough metal surface," J. Opt. Soc. Am. A **18**, 1507–1518 (2001).
8. We have chosen to use the term "enhanced forward scattering," because it is an enhancement in the incoherently scattered light and because "specular scattering" is often understood to mean "coherent scattering."
9. K. A. O'Donnell and E. R. Mendéz, "Enhanced specular peaks in diffuse light scattering from weakly rough metal surfaces," J. Opt. Soc. Am. A **20**, 2338–2346 (2003).
10. I. Simonsen, "Enhanced back and forward scattering in the reflection of light from weakly rough random metal surfaces," Phys. Status Solidi B **247**, 2075–2083 (2010).
11. P. B. Johnson and R. W. Christy, "Optical constants of the noble metals," Phys. Rev. **6**, 4370–4379 (1972).
12. I. Simonsen, "Optics of surface disordered systems: a random walk through rough surface scattering phenomena," Eur. Phys. J. Spec. Top. **181**, 1–103 (2010).
13. A. R. McGurn and A. A. Maradudin, "Perturbation theory results for the diffuse scattering of light from two-dimensional randomly rough metal surfaces," Waves Random Media **6**, 251–267 (1996).
14. G. C. Brown, V. Celli, M. Haller, and A. Marvin, "Vector theory of light scattering from a rough surface: unitary and reciprocal expansions," Surf. Sci. **136**, 381–397 (1984).
15. Lord Rayleigh, "On the dynamical theory of gratings," Proc. R. Soc. London, Ser. A **79**, 399–416 (1907).
16. A. G. Voronovich, *Wave Scattering from Rough Surfaces*, 2nd ed. (Springer-Verlag, 1999), pp. 54–63.
17. A. Soubret, G. Berginc, and C. Bourrely, "Backscattering enhancement of an electromagnetic wave scattered by two-dimensional rough layers," J. Opt. Soc. Am. A **18**, 2778–2788 (2001).
18. A. Soubret, G. Berginc, and C. Bourrely, "Application of reduced Rayleigh equations to electromagnetic wave scattering by two-dimensional randomly rough surfaces," Phys. Rev. B **63**, 245411 (2001).
19. A. A. Maradudin, T. Michel, A. R. McGurn, and E. R. Méndez, "Enhanced backscattering of light from a random grating," Ann. Phys. **203**, 255–307 (1990).
20. I. Simonsen, J. B. Kryvi, A. A. Maradudin, and T. A. Leskova, "Light scattering from anisotropic, randomly rough, perfectly conducting surfaces," Comput. Phys. Commun. **182**, 1904 (2011).
21. T. Nordam, P. A. Letnes, and I. Simonsen, "Numerical simulations of scattering of light from two-dimensional surfaces using the reduced Rayleigh equation," ArXiv 1204.4984 (2012).
22. P. A. Letnes, A. A. Maradudin, T. Nordam, and I. Simonsen, "Calculation of the Mueller matrix for scattering of light from two-dimensional rough surfaces," Phys. Rev. A **86**, 031803 (2012).
23. V. Agranovich and D. Mills, eds., *Surface Polaritons: Electromagnetic Waves at Surfaces and Interfaces* (North-Holland, 1982), pp. 93–145.
24. A. A. Maradudin, ed., *Light Scattering and Nanoscale Surface Roughness* (Springer-Verlag, 2007), pp. 107–126.
25. I. Simonsen, A. A. Maradudin, and T. A. Leskova, "The scattering of electromagnetic waves from two-dimensional randomly rough penetrable surfaces," Phys. Rev. Lett. **104**, 223904 (2010).
26. I. Simonsen, A. A. Maradudin, and T. A. Leskova, "The scattering of electromagnetic waves from two-dimensional randomly rough perfectly conducting surfaces: the full angular intensity distribution," Phys. Rev. A **81**, 013806 (2010).
27. T. Nordam, P. A. Letnes, I. Simonsen, and A. A. Maradudin, "Satellite peaks in the scattering of light from the two-dimensional randomly rough surface of a dielectric film on a planar metal surface," Opt. Express **20**, 11336–11350 (2012).
28. W. H. Press, S. A. Teukolsky, W. T. Vetterling, and B. P. Flannery, *Numerical Recipes: The Art of Scientific Computing*, 3rd ed. (Cambridge University, 2007), pp. 605–608.